Structure, Vol. 11, 43–53, January, 2003, ©2003 Elsevier Science Ltd. All rights reserved. PII S0969-2126(02)00934-6

Comparison of X-Ray Crystal Structure of the 30S Subunit-Antibiotic Complex with NMR Structure of Decoding Site Oligonucleotide-Paromomycin Complex

Stephen R. Lynch,[1] Ruben L. Gonzalez, Jr., and Joseph D. Puglisi*
Department of Structural Biology
Stanford University School of Medicine
Stanford, California 94305

Summary

Aminoglycoside antibiotics that bind to 16S ribosomal RNA in the aminoacyl-tRNA site (A site) cause misreading of the genetic code and inhibit translocation. Structures of an A site RNA oligonucleotide free in solution and bound to the aminoglycosides paromomycin or gentamicin C1a have been determined by NMR. Recently, the X-ray crystal structure of the entire 30S subunit has been determined, free and bound to paromomycin. Distinct differences were observed in the crystal structure, particularly at A1493. Here, the NMR structure of the oligonucleotide-paromomycin complex was determined with higher precision and is compared with the X-ray crystal structure of the 30S subunit complex. The comparison shows the validity of both structures in identifying critical interactions that affect ribosome function.

Introduction

The ribosome is the target of many clinically important antibiotics, which interfere with various steps in the translation cycle. These antibiotics often interact directly with ribosomal RNA (rRNA) in conserved regions that are involved in ribosome function. Aminoglycoside antibiotics bind to an internal loop in helix 44 of 16S rRNA, in a region called the decoding site [1, 2]. This region of the small ribosomal subunit is the site of the codon-anticodon interaction in the aminoacyl-acceptor site (A site) [3], and aminoglycoside binding to helix 44 causes a decrease in translational fidelity [4, 5]. Aminoglycoside binding induces a high-affinity conformation of the ribosome for the codon-anticodon complex [6]; this conformation allows increased selection of incorrect tRNAs within the A site [7].

We have explored the aminoglycoside-rRNA interaction extensively using biochemical, genetic, and structural methods. Chemical probing and mutagenesis on the ribosome and a decoding site model RNA oligonucleotide confirmed the validity of the small oligonucleotide model system for studying aminoglycoside interaction with its ribosomal target [8]. Three NMR solution structures of the eubacterial decoding site oligonucleotide, free in solution and bound to the aminoglycosides paromomycin or gentamicin C1a, were determined [9]. Paromomycin binds in the major groove of an internal loop in the decoding site oligonucleotide that mimics the helix 44 internal loop in 16S rRNA and makes base and backbone contacts that yield sequence specificity. A similar structure is formed by the aminoglycoside gentamicin C1a complexed to the decoding site oligonucleotide [10]. Comparison of the free and aminoglycoside-bound oligonucleotide structures showed that drug binding to the ribosome induced a local conformational change in universally conserved 16S rRNA nucleotides A1492 and A1493, displacing these bases toward the minor groove of helix 44 [11]. Biochemical data subsequently demonstrated the importance of these bases for codon-anticodon recognition in the A site [12]. On the basis of the structural and subsequent biochemical data, we proposed a model whereby A1492 and A1493 read the conformation of the A site codon-anticodon helix and participate directly in the process of selecting cognate over near- or noncognate aminoacyl tRNA [10, 11]. Aminoglycosides induce miscoding by mimicking the conformational change in 16S rRNA induced by a correct codon-anticodon pair.

Recently, the crystal structure of the entire 30S subunit simultaneously bound to three antibiotics, paromomycin, streptomycin, and spectinomycin, was determined in the Ramakrishnan laboratory, demonstrating similarity between the NMR structure of the decoding site oligonucleotide-paromomycin complex and the 30S subunit-paromomycin complex [13]. Unlike most of 16S rRNA, the helix 44 region of 16S RNA that forms the aminoglycoside binding pocket does not interact with any ribosomal proteins or other regions of 16S RNA [13, 14]. This illustrates why using a fragment of rRNA in the NMR studies discussed above recapitulated rRNA structure and function in the intact ribosome and why NMR was successfully used to investigate ribosomal function in this case. The crystallographic studies confirmed the essential features of the model for aminoglycoside-induced miscoding discussed above. However, paromomycin in the 30S structure induces a much larger conformational change in A1492 and A1493. Similarly, the crystal structure of a decoding site oligonucleotide in complex with two molecules of paromomycin recently determined in the Westhof laboratory exhibits essentially the same features as the crystal structure of the complex of the entire 30S subunit and the three antibiotics, including paromomycin [15]. In the decoding site oligonucleotide-paromomycin crystal structure, A1492 and A1493 display a similar large conformational change upon drug binding.

Here, we recalculate the decoding site oligonucleotide-paromomycin complex NMR solution structure with a different force field in order to confirm that the force field used in the original NMR structure calculation protocol did not bias the original structure determined by NMR. In addition, we have measured residual dipolar couplings for the decoding site oligonucleotide-paromomycin complex and recalculated the structure in order to define the global features of the solution structure more precisely and accurately. Finally, we analyze the nuclear Overhauser effect (NOE) crosspeaks observed

*Correspondence: puglisi@stanford.edu
[1]Present address: Department of Chemistry, Stanford University, Stanford, California 94305.

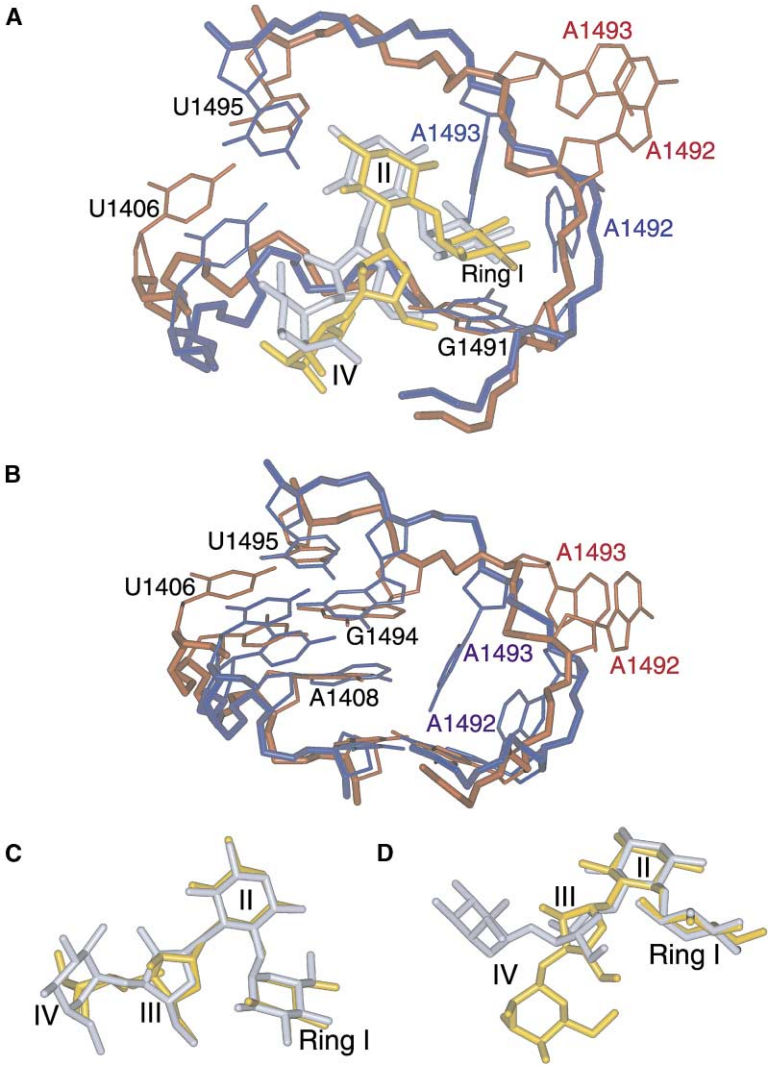

Figure 1. Superposition of the NMR and X-Ray Structures of the Paromomycin-rRNA Complex

The Watson-Crick base pairs of the lower stem (C1409-C1411 and G1488-G1491) are superimposed to compare the relative position of the internal loop (U1406-A1408 and A1492-U1495) and the rings of paromomycin.

(A) The top panel shows the RNA bound to paromomycin.

(B) The bottom panel includes the RNA only, omitting the drug for clarity. The RNA of the NMR structure is blue, with paromomycin in gold; the X-ray structure is red, with paromomycin in silver.

(C and D) The NMR structure of paromomycin (gold) in the complex with the RNA is superimposed on paromomycin (silver) in the X-ray structure. Two different views are shown, demonstrating the difference in position in ring IV. The RNA is not shown for clarity.

in the NMR studies and demonstrate that the crystal structures do not fit all of the NOEs. The differences in the crystal and NMR structures are discussed with important implications for ribosome structure and function.

Results

Comparison of NMR and Crystal Structures

The section of the crystal structure of the 30S subunit bound to the three antibiotics that includes the decoding site-paromomycin complex is compared with the NMR solution structure of the decoding site oligonucleotide-paromomycin complex in Figure 1. The global features of the two structures are quite similar. Paromomycin binds in the major groove of the RNA in the core of highly conserved nucleotides that comprise the decoding site. The RNA forms a binding pocket that fits tightly around the drug, with many intermolecular hydrogen bonds and electrostatic interactions. The ring I of the antibiotic inserts into a pocket in the RNA formed upon displacement of the universally conserved A1492 and A1493 and stacks on top of the base of G1491. Ring II of the drug interacts with the major groove carbonyls of G1494 and U1495. These two nucleotides are base paired to C1407 and U1406, respectively. Ring III projects toward the lower stem from ring II and contacts the base of G1491, positioning ring IV to make further backbone contacts. Ring IV forms hydrogen bonds to the backbone on both sides of the helix, in the lower stem at U1490 and G1491 and across the helix between G1405 and U1406.

In Figure 1, the lower stem residues of the RNA (C1409-C1412 and G1488-G1491) are superimposed to compare the crystal and NMR structures. The backbone, particularly on the U/C1490-C1496 side of the helix, superimposes well. The bases of A1408, C1409, G1491, G1494, and U1495, as well as A/G1410 and U/C1490 (data not shown), also superimpose well in the two structures. The position of paromomycin, particularly rings I, II, and III, superimposes well in the NMR and crystal structures. Three primary differences between the NMR and crystal structures are as follows: (1) the position of ring IV of paromomycin, (2) the position of the bases of U1406 and C1407 along with the backbone in the vicinity of those nucleotides, and (3) the position of the bases

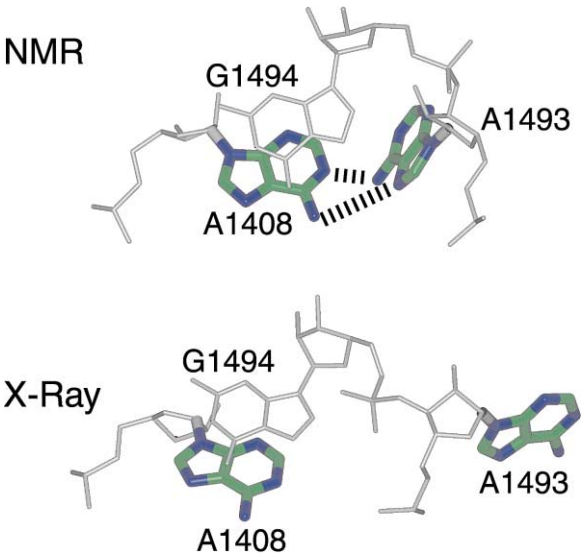

Figure 2. The Positions of A1408, A1493, and G1494 Are Compared in the NMR and X-Ray Structures of the Paromomycin-rRNA Complex

A base pair was observed in the NMR structure between A1493 and A1408, with hydrogen bonds (shown with dashes) from the N1 of A1408 to the amino proton of A1493 and from the amino proton of A1408 to the N7 of A1493. No base pair is observed in the X-ray structure, as A1493 is displaced further toward the minor groove.

of A1492 and A1493. The difference between ring IV of paromomycin in the NMR and crystal structures is not significant, as ring IV was clearly disordered in the family of low-energy NMR structures, whereas the crystal structure selects a single conformation. The difference at U1406 and C1407 is also insignificant, as the overall helical geometry for these two nucleotides and the U1406-U1495 and C1407-G1491 base pairs is similar in the two structures. U1406 and C1407 are stacked in both structures. The difference is essentially in the global bending of the structure that takes place at the assymetric internal loop in the vicinity of the U1406-U1495 and C1407-G1491 base pairs. Global bends are difficult to detect with NMR, as long-range constraints do not exist. In the range of low-energy structures consistent with the NMR data, bend angles of the helix vary. Even small differences in backbone angles throughout the stem in the NMR structures are propagated to create the range of helical bend angles observed.

The positions of A1492 and, particularly, A1493 are the major difference between the crystal and NMR structures. In the NMR structure, the bases of A1492 and A1493 are displaced toward the minor groove upon binding to paromomycin, but they are still within the binding pocket. In the crystal structure, the two bases are completely flipped out of the helix, not making contact to any part of the drug or any part of the 30S subunit. Additionally, it is only the bases of the two residues that are different; the backbone is almost identical. The difference in the position of the base A1493 is further highlighted in Figure 2. In the NMR structure, a base pair is observed between A1408 and A1493. The N6 amino protons of A1408 form a hydrogen bond to the N7 of A1493, and the N6 amino protons of A1493 form a hydrogen bond to the N1 of A1408. In the crystal structure, the two bases are much too far apart for hydrogen bonds. Since the position and orientations of G1494 and A1408 are quite similar in the two structures, only A1493 and A1492 differ between the two structures.

The published crystal structure is the entire 30S subunit with three separate drugs, including paromomycin. Although the NMR construct of the decoding site includes only 19 nucleotides from 16S rRNA, the entire binding pocket for paromomycin is within the oligonucleotide. Additionally, no other rRNA or protein density is observed in the crystal structure at or near the paromomycin binding site. However, streptomycin, a second antibiotic in the crystal structure, makes van der Waals contact and hydrogen bonds to some of the same nucleotides that paromomycin is contacting. Streptomycin increases the affinity of paromomycin for the ribosome. However, streptomycin binding does not cause the observed structural differences discussed above, as the rRNA structure observed in a decoding site oligonucleotide crystal structure in the presence of only paromomycin [16] is essentially the same as that in the 30S subunit-three antibiotic complex.

Comparison of the Paromomycin Structure in the X-Ray and NMR Structures

The structures of paromomycin in the crystal and NMR structure are compared in Figure 1. Rings I and II adopt identical chair conformations in the crystal and solution structures. Ring III adopts a C_2'-*endo* conformation in the crystal structure, but a C_3'-*endo* conformation in the NMR structure. The difference in the conformation of ring III is transmitted to ring IV, affecting its position. Ring IV is in a chair conformation in both the crystal structure and the average NMR structure, but the type of chair conformation is different. In the crystal structure the 2‴, 3‴, and 4‴ heavy atoms are found in axial positions. The average NMR structure has the 2‴, 3‴, and 4‴ heavy atoms in equatorial positions, with the C6‴ and oxygen-linking rings III and IV in axial positions. Ring IV is clearly disordered and adopts various conformations in the family of NMR structures (rmsd of 0.40 Å among the 19 final structures). The disorder of ring IV in the NMR structures is in agreement with the narrow line widths of the ring IV protons compared with the line widths of the protons on rings I and II. Although ring IV adopts various conformations, the exact conformation of ring IV in the crystal structure is not observed in any member of the family of low-energy NMR solution structures.

Intermolecular RNA-Paromomycin Contacts

The intermolecular contacts and paromomycin-paromomycin contacts observed in the crystal and NMR structures of the 30S subunit and decoding site oligonucleotide bound to paromomycin, respectively, are compared in Table 1. Paromomycin-paromomycin or paromomycin-RNA base, rather than paromomycin-RNA phosphate contacts are most similar in the two structures and are also the most precise in the family of low-energy NMR structures. The contacts that are least similar be-

Table 1. Comparison of Intermolecular Contacts in X-Ray Crystal Structure and NMR Structure

	Distance in Crystal Structure of 30S Subunit-Drug Complex (Å)	Distance in NMR Structure of RNA Oligonucleotide-Paromomycin Complex (Å)
Ring I O3′-A1492 O1P	3.1	3.9 ± 0.6
Ring I O4′-A1493 O1P	2.5	3.7 ± 0.6
Ring I O6′-A1408 N1	2.7	4.8 ± 0.6
Ring I O6′-A1493 O1P	5.0	4.1 ± 0.7
Ring I N2′-Ring III O4″	2.6	2.7 ± 0.1
Ring I N2′-Ring III O5″	2.4	4.1 ± 0.5
Ring II N2-G1494 O1P	2.6	5.9 ± 0.3
Ring II N2-G1494 N7	3.0	3.3 ± 0.1
Ring II N4-U1495 O4	2.7	3.1 ± 0.1
Ring III O5″-G1491 N7	2.4	3.3 ± 0.5
Ring IV N6‴-U1490 O1P	2.5	8.1 ± 0.8
Ring IV O4‴-G1405 O1P	3.4	7.0 ± 0.5
Ring IV O3‴-G1405 O2P	2.2	6.7 ± 0.8
Ring IV N2‴-U1406 O1P	3.6	3.7 ± 0.6
Ring IV N2‴-Ring III O2″	2.5	5.2 ± 0.3

tween the crystal and NMR structures are those of ring IV of paromomycin, which samples multiple conformations and is therefore poorly defined in the NMR structure. There are two additional differences, aside from those from ring IV, in the crystal and NMR structures. These are the contact of the ring I 6′ OH to the N1 of A1408 and the contact of the N3 of ring II to the phosphate oxygen of G1494. Similar to that on ring IV, the 6′ position on ring I is not well defined in the NMR structure. Furthermore, an A1408-A1493 base pair is observed in the NMR structure, with the N1 of A1408 hydrogen bonding to the A1493 amino proton; in the crystal structure, the 6′ OH hydrogen bonds to the A1408 N1. The ring II N3 to G1494 phosphate oxygen is also quite different between the crystal and NMR structures. The phosphate of G1494 is positioned toward paromomycin in the crystal structure, whereas the ribose and base of A1493 occupy this space in the NMR structure.

NOE Violations of Crystal Structure

The crystal structure of the 30S subunit-paromomycin complex was analyzed to determine the number and magnitude of violations to proton-proton NOE distance constraints determined by NMR. Molecular modeling was used to build hydrogen atoms into the crystal structure. The distances between protons were then compared to the distance constraint file used for structure calculation on the basis of the NMR data. Out of 452 NOEs, a total of 65 NOEs were violated by the crystal structure, 36 out of 392 RNA-RNA, 4 out of 12 paromomycin-paromomycin, and 25 out of 48 RNA-paromomycin NOEs. Out of the 65 NOE violations, the 23 with most significant distance violations (>0.9 Å) are presented in Table 2. All of the large violations of RNA-RNA NOEs by the crystal structure involve the position of A1493, with the largest violations related to the presence (in the NMR structure) or absence (in the crystal structure) of an A1408-A1493 base pair. The other RNA-RNA violations result from different positions of the ribose moiety of A1493. While the RNA backbone from A1492 to G1494 is essentially the same, the ribose heavy atoms of A1493 that are not directly part of the phosphodiester backbone (O4′, C1′, and C2′) are flipped out in the crystal structure (Figure 1). Additionally, while the C3′ of A1493 is similar in the two structures, the H3′ points in different directions, resulting in the NOE violations from the H3′ of A1493.

Intermolecular NOEs represent the largest percentage of significant NOE violations (14 of 48 versus 8 of 392 RNA-RNA NOEs and 1 of 12 paromomycin-paromomycin NOEs). Six of the 14 intermolecular NOE violations, including the 2 largest, involve A1492 and A1493. Six more of the 14 involve the dynamic ring IV. The remaining two violations involve exchangeable protons on the RNA. Since ring IV is dynamic in the NMR structure, but static in the crystal structure, NOE violations to ring IV are not surprising. Protons from ring IV are transiently in close proximity to protons on the RNA, resulting in observed NOEs, even though individual structures suggest that those protons are too far apart. The NOE violations to the two exchangeable resonances on the RNA are also not surprising, as NOEs to exchangeable protons are often hard to quantify because of the long mixing times required to observe the intermolecular NOEs and the solvent exchange of the proton.

Position of A1493

NOESY data were acquired on the decoding site oligonucleotide-paromomycin complex to confirm the presence or absence of an A1493-A1408 base pair on the basis of the significant difference in the X-ray crystal structure and NMR solution structure. As shown in Table 2, eight RNA-RNA NOEs are violated by the crystal structure, all related to the position of A1493. These are mostly due to the position of the A1493 base relative to A1408, but, also, there are three RNA-RNA NOEs related to the A1493 ribose, as it is flipped out in the crystal structure, as well. Figure 3A presents a ^{13}C-filtered NOESY spectrum acquired on a decoding site oligonucleotide-paromomycin complex sample where only the adenosine residues were $^{13}C/^{15}N$ labeled. Only NOEs resulting from adenosine protons bound to carbons are observed to resolve overlap in a standard NOESY spectrum. A clear, unambiguous NOE from A1493 H2 to C1409 H1′ is shown in Figure 3A. While this NOE does not confirm that there is a base pair at room temperature in solution for the decoding site RNA bound to paromomycin, it does confirm that the two protons are close in

Table 2. Proton-Proton NOEs Violated by X-Ray Crystal Structure of 30S Subunit Complex

Atom 1	Atom 2	Distance in 30S (Å)	Distance Violation to NMR Constraint (Å)
A1408 H2	A1493 H2	13.7	8.1
A1408 H2	A1493 N6	11.3	6.8
A1408 N6	A1493 N6	13.9	8.9
A1408 N6	A1493 H8	10.1	5.5
A1493 H3′	A1493 H8	2.2	−1.3
A1493 H2′	G1494 H8	5.9	3.3
A1493 H3′	G1494 H8	4.4	0.8
A1493 H2	C1409 H1′	14.9	9.4
G1494 NH	U1406 NH	5.5	0.5
Ring III H1‴	Ring I H3′	6.3	1.3
A1492 H3′	Ring I H4′	6.1	1.1
A1493 H8	RIng I H4′	7.3	1.3
A1493 H8	Ring II H2eq	8.2	3.2
A1493 H3′	Ring II H2ax	6.0	1.0
G1494 NH	Ring II H2ax	6.8	0.9
A1493 H2′	Ring II H3	8.1	2.6
A1492 H3′	Ring II H3	5.9	0.9
U1406 NH	Ring II H6	7.2	1.2
U1406 H5	Ring IV H1‴	6.1	1.1
U1406 H6	Ring IV H4‴	7.7	1.7
C1490 H5	Ring IV H3‴	7.2	2.2
G1489 H8	Ring IV H4‴	7.6	1.6
C1490 H5	Ring IV H4‴	7.5	2.5
C1490 H5	Ring IV H6‴	6.0	1.0

space for a significant amount of time in the complex. These two protons are 14.9 Å apart in the crystal structure; thus, no A1493 H2-C1409 H1′ NOE would be observed for the RNA conformation in the crystal structure. The crystal structure conformation could exist for a small percentage of time in solution, but the major solution conformation must have the base of A1493 close to the helix.

The ribose of A1493 is flipped out in the crystal structure, but not in the NMR structure. Figure 3B shows the ribose region of the same NOESY spectrum in Figure 3A. The NOE from the H3′ of A1493 to the H8 of A1493 is highlighted. In the crystal structure, these two protons were 2.2 Å apart, which would lead to a very intense NOE, one of the most intense in the spectrum, as few protons are that close in RNA. Although a NOE is observed, it is not one of the most intense in the spectrum. Although other factors, such as line width and relaxation, can affect NOE intensity, these factors alone cannot account for the discrepancy. This NOE should still be the most intense for both the H3′ and the H8 of A1493 if the crystal structure conformation was predominant in the decoding site oligonucleotide in solution.

Residual Dynamics in the Paromomycin-RNA Complex

The RNA and paromomycin moieties at the RNA-drug interface show evidence of microsecond to millisecond exchange dynamics in the NMR structure. Resonances for the ring I 6′ and 2′ protons are significantly broadened, as is the A1408 H8 resonance. Broadening of these resonances is caused by conformational exchange processes on the microsecond to millisecond timescale; in contrast, no evidence for exchange broadening is observed for A1492 and A1493. These qualitative observations highlight the dynamic nature of the decoding site oligonucleotide-paromomycin complex.

Recalculating NMR Structures with X-PLOR

The structure of the decoding site oligonucleotide-paromomycin complex was recalculated with X-PLOR [17]; the original structures were calculated with the DISCOVER 3 force field within Insight II (Molecular Simulations, San Diego, CA) (Fourmy et al., 1996). The force fields of the two programs are different, and the calculation protocol is also different. Recalculation of the structure was carried out in order to confirm that calculation protocols and/or force fields are not biasing the NMR-determined structure. In addition to the use of a different calculation protocol and force field, NOE-derived distance constraints were loosened relative to the original structure calculation to allow for any possible discrepancies in the conversion of NOE volumes to proton distances. A comparison of the X-PLOR recalculated structures to the crystal structure is presented in Figure 4. The position for all nucleotides except A1492 and A1493 are within the range of low-energy recalculated structures. The position of A1492 in the recalculated structures is not as well defined as other nucleotides, and its position approaches that observed in the crystal structure. The dynamics of A1492 were not noted in the original description of the NMR structure of the decoding site oligonucleotide-paromomycin complex [9]. Either the difference in the forcing energies of DISCOVER 3 versus X-PLOR or the tighter NMR-derived constraints in the original DISCOVER 3 calculations apparently overconstrained the base of A1492 to a better-defined position in the original DISCOVER 3-derived structures. However, even in the recalculated structures, A1493 does not approach its position in the crystal structure.

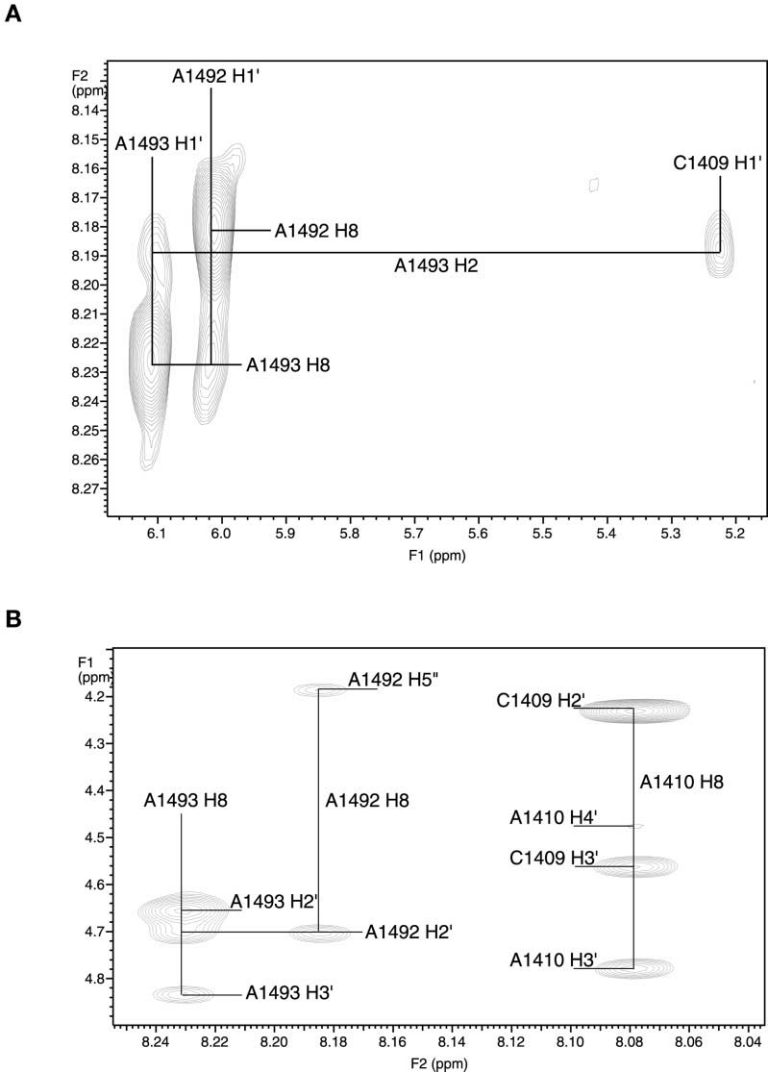

Figure 3. Direct NMR Data Confirms that the Position of A1493 Observed in the NMR Structures Is the Major Solution Conformation for This Nucleotide

(A) The aromatic H1′ region of a ($^{13}C/^{1}H$) HSQC-NOESY acquired on a specifically $^{13}C/^{15}N$-labeled RNA (adenosines only) decoding-site oligonucleotide-paromomycin complex is presented. Since the sample is specifically labeled, the only NOEs observed are those from adenosine residues (A1408, A1410, A1492, and A1493). The NOE between C1409 H1′ (5.22 ppm) and A1493 H2 (8.19 ppm) is highlighted. The NOESY spectrum was acquired on a Varian 800 MHz spectrometer, with sweep widths of 8000 Hz in each dimension, 1024 complex points in F2, 512 complex points in F1, 32 scans per increment, a relaxation delay of 2.0 s, and a mixing time of 250 ms. The matrix was zero filled to 2048 × 2048. (B) The aromatic/ribose region of the same NOESY is presented. Note the moderate intensity NOE between the A1493 H3′ and the A1493 H8 in contrast to the much more intense NOEs between A1493 H2′ and A1493 H8 and between C1409 H2′ and A1410 H8, indicating that the A1493 H3′ is not very close to the A1493 H8.

Refining NMR Structures with Residual Dipolar Couplings

The structure of the decoding site oligonucleotide-paromomycin complex was refined against 37 residual dipolar coupling restraints with the CNS force field [18], starting with the original DISCOVER 3 structures. The structure statistics for the refinement are presented in Table 3. Of the 19 original structures, 13 converged to low energy with the additional constraints from the residual dipolar couplings. The final refined and energy-minimized structures calculated with residual dipolar couplings are presented in Figure 5. The overall precision of the structure is much higher with the additional constraints from the residual dipolar couplings (rmsd = 0.52 ± 0.18 Å). Additionally, the precision of the structure in the core region interacting with paromomycin (G1405-A1410 and U1490-C1496) is much higher (rmsd = 0.34 ± 0.16 Å). The only nucleotide that is part of the 16S rRNA sequence that is not well defined in the new structures with residual dipolar coupling restraints is A1492. The base of A1492 is dynamic in the calculated structures, again approaching its position in the crystal structure.

The original DISCOVER 3 NMR structure of the decoding site oligonucleotide-paromomycin complex is compared to the structure refined with residual dipolar couplings in Figure 6. Globally the structures are essentially the same. Structures refined with residual dipolar couplings have a more precise bend angle between the two helical stems, since residual dipolar couplings provide long-range global restraints. The interhelical bend angle in the original DISCOVER 3-derived structures is 131 ± 23°, whereas, in the residual dipolar coupling-refined structures, it is 131 ± 12°. In the crystal structure this interhelical bend angle is 163°. In addition to the differences in the interhelical bend angles, the residual dipolar coupling-refined structures are also elongated relative to the original NMR structures. The longest phosphate to phosphate distance in the original NMR structures is 32 ± 4 Å. In the residual dipolar coupling-refined structures, this distance is 37 ± 1 Å. The equivalent phosphate to phosphate distance in the crystal structure is approximately 40 Å. As expected, the residual dipolar coupling restraints improve the precision of the NMR structures. This is particularly true for global structural

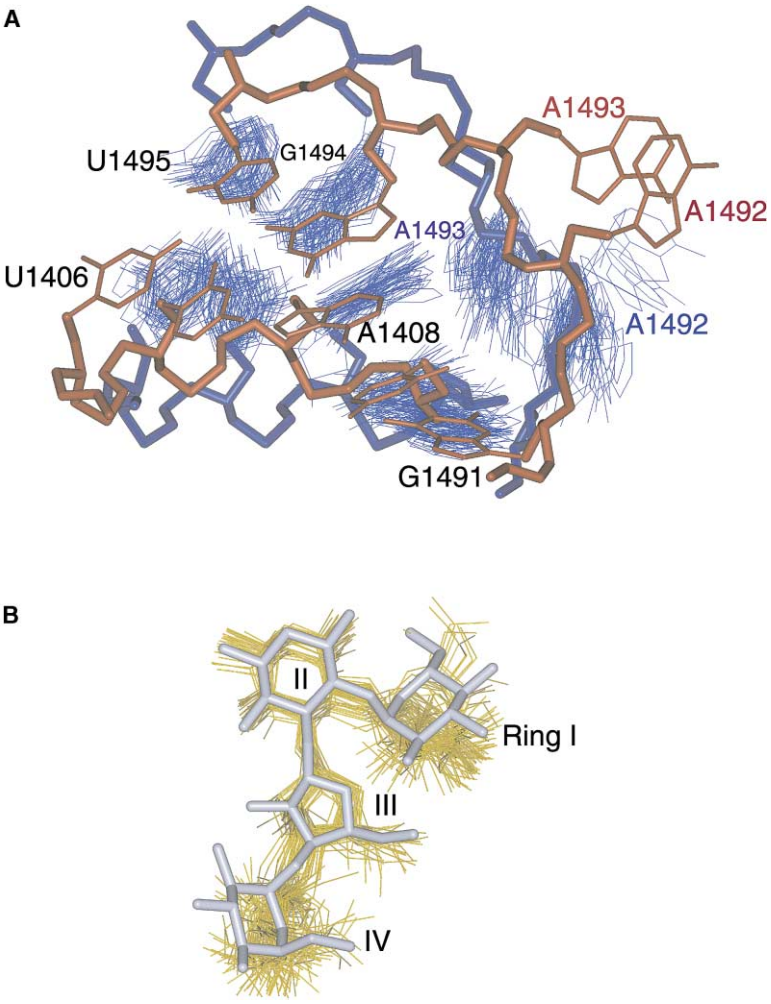

Figure 4. Comparison of the Decoding Site NMR Structure Recalculated with the XPLOR Force Field and the Decoding Site from the Crystal Structure of the 30S Ribosomal Subunit

(A) NMR structures were recalculated in X-PLOR with loose distance constraints. The lower stem (C1409-C1411 and G1488-G1491) of the X-ray structure (red) is superimposed on the minimized average structure of the recalculated NMR structures (blue). Structures were recalculated from 100 starting structures; the 35 lowest energy structures were refined and minimized and are presented in this figure. Only the bases of U1406-C1409 and G1491-U1495 are shown.

(B) Paromomycin of the X-ray structure (silver) is superimposed on the NMR structures calculated with XPLOR (gold).

features such as the interhelical bend angle and the overall length of the NMR structure.

The structures refined against residual dipolar couplings are compared with the crystal structure of the 30S subunit-paromomycin complex in Figure 7. The core nucleotides interacting with paromomycin are in similar positions in the crystal structure and the structures refined with dipolar couplings, except for the bases of A1492 and A1493, as observed in the previous NMR and crystal structure comparisons. The base of A1492 is in several conformations in the dipolar coupling-refined structure, consistent with dynamic nature of this nucleotide, and with the flipped-out conformation observed in the crystal structure. However, A1493 is well defined, and again not close to its position in the crystal structure.

Table 3. Structure Statistics and Atomic Rms Deviations

Final forcing energies (kcal/mol)	
Distance, dihedral, and dipolar coupling	27.7 ± 0.5
Rmsd from distance constraints (Å)	
All (382)	0.28
Rmsd from dihedral constraints (°)	
All (106)	0.83
Rmsd from residular dipolar coupling constraints (Hz)	
All (37)	1.23
Deviations from idealized geometry	
Bonds (Å)	0.0036
Angles (°)	0.80
Impropers (°)	0.47
Heavy atom rmsd	
All	0.52
Core residues and paromomycin	0.34

Discussion

Reductionism is a common theme in structural biology; this is particularly true with RNAs, which tend toward large, multicomponent complexes. The comparison of the RNA-aminoglycoside complexes determined with a 27 nt decoding site oligonucleotide RNA (10 kDa) and the entire 30S ribosomal subunit (800 kDa) shows the validity and limitations of reductionism. The deoxystreptamine-containing aminoglycosides bind in the major groove of an asymmetric internal loop in helix 44 of 16S rRNA; this type of structure is readily recapitulated by an RNA oligonucleotide. The RNA-aminoglycoside interactions observed in the two structures are similar, as anticipated by comparative mutational studies performed in the decoding site oligonucleotide and in the

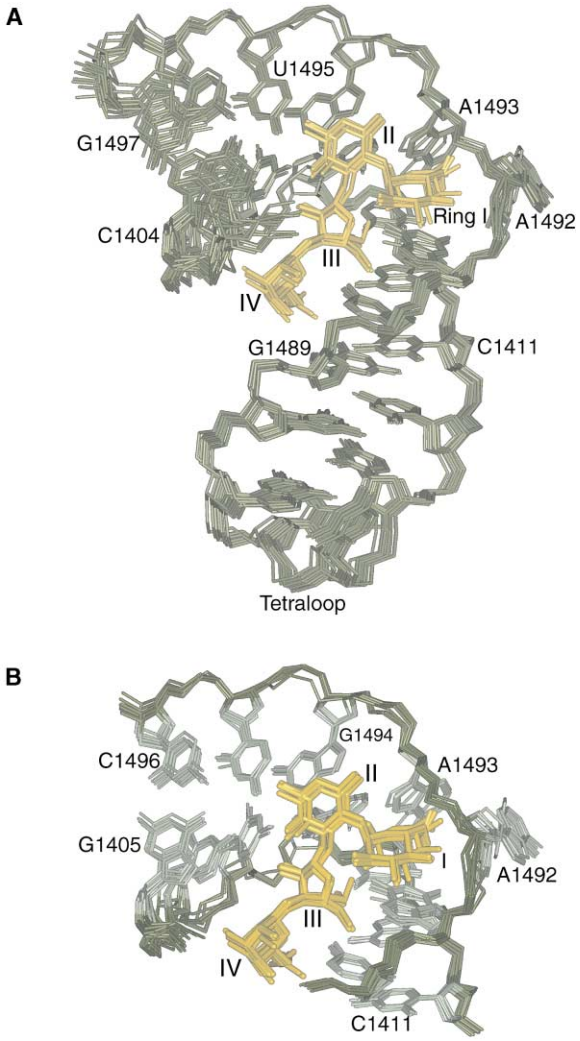

Figure 5. The Final Energy-Minimized Decoding Site NMR Structures Refined against Residual Dipolar Couplings

(A) Overall superposition of 14 structures refined with residular dipolar couplings. RNA, green; paromomycin, gold. The overall rmsd for the 14 structures shown was 0.52 Å.

(B) The bases of the core region of the RNA are highlighted with ribbons depicting the phosphodiester backbone of the RNA-paromomycin complex refined with residular dipolar couplings.

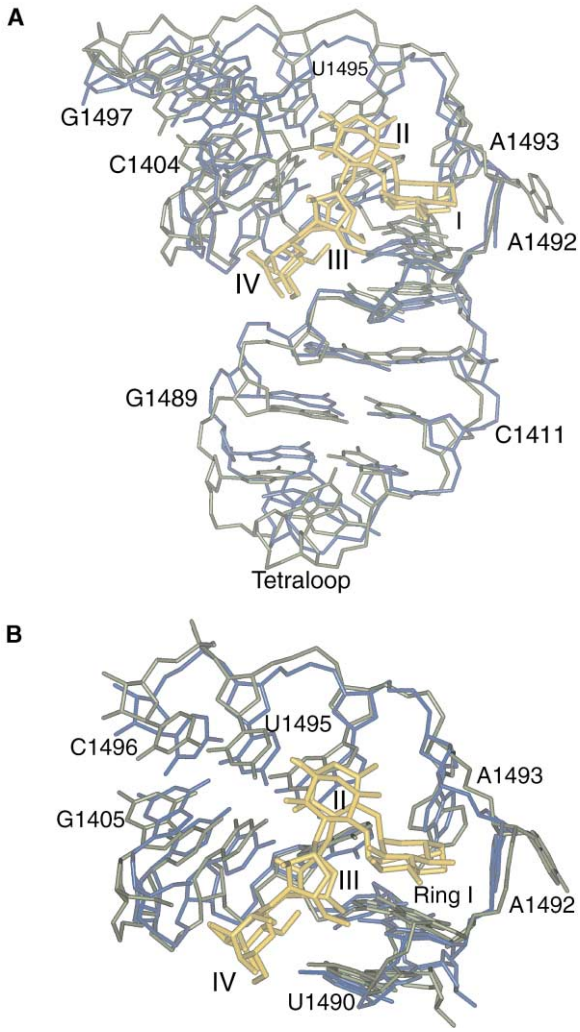

Figure 6. A Comparison of the Original Decoding Site Oligonucleotide-Paromomycin NMR Structure with One Structure of the Family Refined with Residual Dipolar Couplings

(A) The overall structures are compared, with the RNA of the original structure in blue and paromomycin in gold, while the structures refined with dipolar couplings are green (RNA), with paromomycin in gold.

(B) The core region of the original NMR structure and the dipolar coupling-refined structure are compared.

ribosome [8]. Confidence in the validity of a reduced RNA system is established by rigorous genetic, biochemical, and biophysical comparisons of the model and intact system. In contrast to paromomycin, streptomycin binds to a complex rRNA structure in the 30S subunit, with ribosomal protein S12 contributing to the drug binding site [13]. Despite the local nature of the RNA-ligand interaction, an RNA-drug complex such as that with streptomycin could not be readily recapitulated into a model system.

Residual dipolar coupling measurements provide constraints on global RNA conformation. Refinement of the original NMR structures of the decoding site oligonucleotide-paromomycin complex was performed with additional residual dipolar coupling restraints. First, the structure of the complex was recalculated with X-PLOR without residual dipolar couplings. There was little effect of the change of force field and calculation protocol on the final structures. Finally, the structures were refined against residual dipolar couplings. This led to an improvement in the overall rmsd of the final structures and improvements in the precision of global structural features such as the interhelical bend angle and the overall length of the structures. Paromomycin binding induces a larger conformational change in A1492 and A1493 in the crystal structure of the 30S subunit than in the NMR structure of the decoding site oligonucleotide [13–15].

The X-ray crystal structure of a decoding site oligonucleotide-paromomycin complex has been recently determined at higher resolution (2.5 Å) than that of the 30S subunit-paromomycin complex [15]. As in the NMR structures, the decoding site oligonucleotide-paromo-

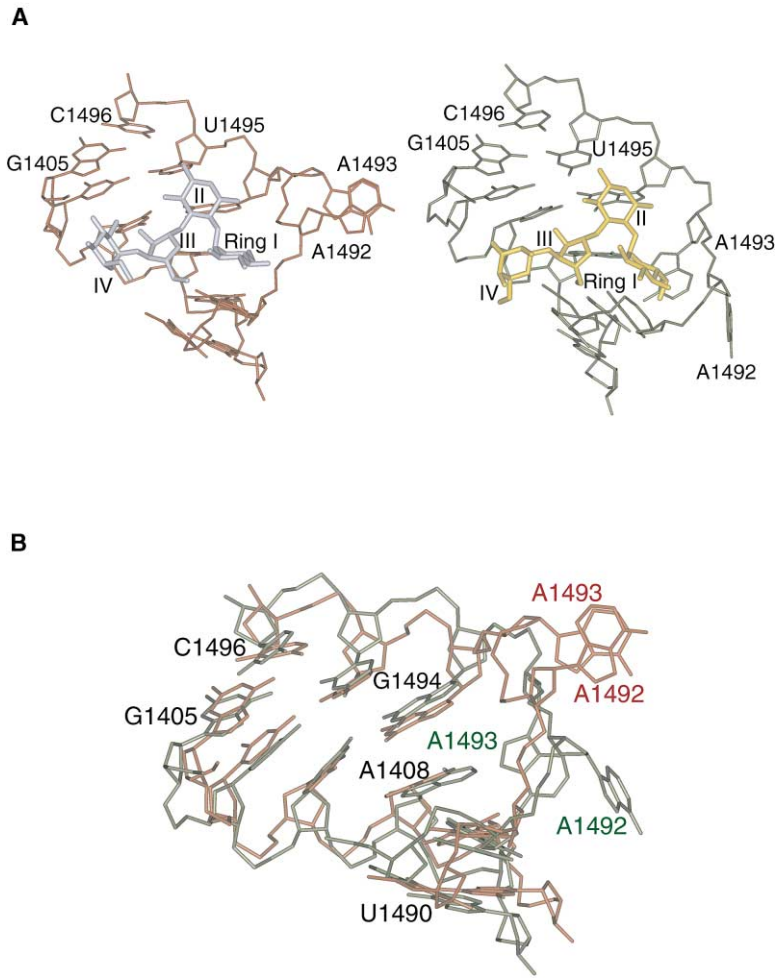

Figure 7. A Comparison of the 30S Subunit-Paromomcyin Crystal Structure with the Superposition of NMR Structures Refined with Residual Dipolar Couplings

Only the core region of the structures are shown, with the RNA of the dipolar coupling-refined structures in green and paromomycin in gold, whereas the RNA of the crystal structure is red, with paromomycin in silver.

(A) Side by side comparison of the RNA-drug complexes.

(B) Superposition of the RNA. The drug has been omitted for clarity.

mycin contacts observed are similar to those observed in the entire 30S subunit-paromomycin complex, but, at the higher resolution achieved for the decoding site oligonucleotide, contacts through bound water molecules were more easily discerned from direct contacts. As in the 30S crystal structure, ring I of paromomycin displaces A1492 and A1493 toward the minor groove of the RNA in the decoding site oligonucleotide-paromomycin crystal structure. The extrusion of A1492 and A1493 in this crystal structure is stabilized by intermolecular packing interactions of the two adenosines into the minor groove of a neighboring helix. The A site of the 30S subunit crystal structure is also in an environment that is rich in RNA. The NMR data are inconsistent with the presence, at 300–310 K, of a significant population of the conformation of the decoding site observed in the crystal; the crystallographic data for both the 30S subunit-paromomycin complex and the decoding site oligonucleotide-paromomycin complex were acquired in vitreous ice at 100 K. The lower temperature would, at a minimum, dampen conformational dynamics and could shift local conformational equilibria.

Biological Implications

All aminoglycoside antibiotics that bind to the decoding site have a hydrogen bond donor at the 6′ position on ring I. In the crystal structure of the 30S subunit-paromomycin complex and the decoding site oligonucleotide-paromomycin complex, the 6′ OH hydrogen bonds to the N1 of A1408, whereas, in the NMR structure, a 6′ OH- A1493 phosphate oxygen contact is observed. The 1408 position is an adenosine in all prokaryotic sequences and a guanosine in all eukaryotic cytosolic sequences [19]. Mutation of A1408 to G confers high-level resistance to all of the aminoglycosides, except those with a 6′ OH group [20]. Structural studies in solution suggested that a G1408-A1493 base pair disrupts the binding site for the drug, and a 6′ amino group is unable to hydrogen bond the phosphate backbone at A1493 [21]. Mutation of A1408 to G stabilizes the conformation of the internal loop. As suggested by Vicens and Westhof (2001), aminoglycosides with a 6′ OH interact with higher affinity to G1408 ribosomes than do aminoglycosides with a 6′ NH_2 because the N1 imino proton can still hydrogen bond to the 6′ OH, but not to the 6′ NH_2. However, the distorted binding pocket in the solution structure of the G1408 decoding site oligonucleotide suggests why all aminoglycoside bind to G1408 sequences with reduced affinity: the G1408-A1493 base pair disrupts the binding site for the drugs.

The differences in the crystal and NMR structures are real and have implications for aminoglycoside binding and action on the ribosome. Aminoglcyoside binding at

the decoding site displaces A1492 and A1493 toward the minor groove. A1492 is no longer stacked within the helix and is very dynamic, as reflected in the NMR structures. Presumably, A1493 still interacts with A1408, but the N1 position of A1493 is free to interact in the minor groove of the RNA. The crystal structure likely represents the endpoint conformation of the rRNA-paromomycin complex; this conformation is stabilized by interaction of A1492 and A1493 with the RNA minor groove of the tRNA anticodon-mRNA codon helix [13, 14, 16] and interaction with G530. However, the 30S subunit-paromomycin complex is very likely dynamic at physiological temperatures, as is evidenced in the NMR structural studies.

Local conformational dynamics may play a significant functional role in the active centers of the ribosome. Antibiotics that target the ribosome may act by interfering with conformational dynamics that are required for function. Movement of A1492 and A1493 toward the tRNA anticodon-mRNA codon helix may trigger the signaling pathway that relays the acceptance of a codon-anticodon interaction from the decoding site on the small ribosomal subunit to the GTPase and/or peptidyl transferase center(s) of the large ribosomal subunit. Aminoglycosides would induce this signaling, even in the presence of noncognate tRNA. Conformational dynamics of the decoding site are functionally important, and the effect of antibiotics on these conformational dynamics has implications for the design of new antibiotics.

The comparison of the crystal and NMR structures of the RNA-paromomycin complex reveals the validity of both structures and highlights the importance of multiple structure determinations to obtain full understanding of biological systems. These investigations show the strengths and limitations of reductionism in biology.

Experimental Procedures

NMR Sample Preparation

Milligram quantities of the decoding site oligonucleotide were prepared both uniformly $^{13}C/^{15}N$ labeled and selectively $^{13}C/^{15}N$ labeled at the adenosine positions only. The RNAs were in vitro transcribed from an oligonucleotide DNA template and purified as described [22]. After electroelution and ethanol precipitation, the RNA pellet was resuspended in 10 mM sodium phosphate and 20 μM EDTA (pH 6.4). The sample was then dialyzed against the phosphate buffer with a stepwise decrease in sodium chloride from 1 to 0 M in a microdialysis apparatus with a 1000 MW cutoff membrane. The final buffer condition used for NMR experiments was 10 mM sodium phosphate (pH 6.4). The RNA concentration was 1.5 mM in 225 μl in a Shigemi NMR tube. Pf1 phage was added to the NMR sample at a concentration of ~21 mg/ml to achieve partial alignment of the decoding site oligonucleotide-paromomycin complex and to measure residual dipolar couplings.

NMR Spectroscopy

NMR experiments were acquired on either a Varian Inova 800 MHz or Varian Inova 500 MHz spectrometer with triple-resonance and three-axis gradient capabilities. NMR data were processed with VNMR (Varian). Standard $^{1}H/^{1}H$ NOESY, DQF-COSY, and TOCSY experiments were used to confirm previous resonance and NOE assignments of the decoding site oligonucleotide-paromomycin complex. A heteronuclear 2D (^{13}C)-edited NOESY experiment [23] was acquired at 25°C with a mixing time of 250 ms. Three-dimensional HCCH-TOCSY [24], 3D HCP [25], 2D $^{1}H/^{31}P$ heteronuclear COSY [26], and 2D HCCH-TOCSY [27] were used to confirm all resonance assignments on the adenosine residues.

$^{13}C/^{1}H$ residual dipolar couplings were measured with a 2D ^{1}H-coupled sensitivity-enhanced $^{13}C/^{1}H$ HSQC. The spectra acquired were 64 scans of 2048 complex points in t2 by 256 in t1, with a ^{1}H spectral width of 5000 Hz and a ^{13}C spectral width of 3750 Hz. The data were zero filled to 4096 points by 4096 points. $^{15}N/^{1}H$ dipolar couplings were measured with a 2D ^{1}H-coupled sensitivity-enhanced $^{15}N/^{1}H$ HSQC. The spectra acquired were 32 scans of 2048 complex points in t2 by 128 in t1, with a ^{1}H spectral width of 5000 Hz and a ^{15}N spectral width of 1500 Hz. The data were zero filled to 4096 points by 1024 points.

Structure Calculation without Residual Dipolar Couplings

Structures were calculated on the decoding site oligonucleotide-paromomycin complex by restrained molecular dynamics and then energy minimization with the program X-PLOR on an SGI Octane workstation. Random starting structures were created by randomizing backbone torsion angles. The structure calculation was carried out in three stages. The initial stage was a modified simulated-annealing protocol [28] utilizing a force field consisting of bond lengths, bond angles, improper angles, repulsive van der Waals potentials, and experimental distance and dihedral constraints in the absence of electrostatics. For this initial stage, all of the experimental distance constraints were used, but only the dihedral constraints that specified sugar puckers and kept amino groups in the plane of the base pairs were included. Structures that converged to low total energy were subjected to a second-stage refinement protocol that added to the force field described above the experimentally determined backbone dihedral constraints. The structures were then minimized during the third stage of the calculation protocol by adding to the force field attractive Lennard-Jones potentials and electrostatics. The final structures were displayed with the program Insight II (Molecular Simulations, San Diego, CA). Out of 100 starting structures, 35 converged to low energy during the initial stage; these structures were refined and minimized.

Several slight changes were made to the experimental constraints used for this structure calculation compared with the originally calculated structure (Fourmy et al., 1996). Distance constraints from the previous structure determination of the decoding site RNA-paromomycin complex were used, but the ranges for strong, medium, and weak were loosened to 1.8–3.0 Å, 2.5–4.0 Å, and 3.0–6.0 Å, respectively. Similarly, dihedral constraints from the previous structure determination were used, but no modifications were made to the torsion angle ranges. Only experimentally determined torsion angles were used in the calculation; neither backbone torsion angle α nor ζ was constrained at any stage of the calculation.

Structure Calculation with Residual Dipolar Couplings

The final 19 minimized structures of the originally determined RNA decoding site oligonucleotide-paromomycin complex [9] were refined with constraints on the basis of the measured residual dipolar coupling data, in addition to the same distance and dihedral constraints described above, with the program CNS [18]. The force constant for the dipolar coupling constraints were gradually ramped into the calculation over 40 steps at 1000 K, from 0 to a final value of 0.2. The bath temperature was then slow-cooled back to 300 K in 25° steps. Initial values for the axial (D_A) and rhombic components (D_R) of the molecular alignment tensor were determined by application of the Orderten SVD program [29]. The final values for D_A and D_R used in the calculation were determined by varying the values of D_A and D_R and searching for the values that gave a minimum energy with three of the final low-energy structures determined without residual dipolar couplings. The minimum energy values of D_A and D_R from each of the three structures were then averaged and used in the full refinement. The value used for D_A was 22, and the value used for D_R was 0.2. Residual dipolar coupling measurements from structurally dynamic nucleotides were not used as constraints to eliminate the contribution of dynamics to the measured residual dipolar coupling. A total of 37 residual dipolar couplings were used in the calculation. These included dipolar couplings for nucleotides in the two helical stems, with the exception the first base pair, and the three well-defined nucleotides of the UUCG tetraloop. A harmonic potential was used to incorporate the dipolar coupling constraints into the force field. A total of 14 of 19 structures con-

verged to low final energy; the other 5 structures diverged to high energy upon refinement with dipolar couplings and were discarded. Each of the final 14 structures had 35 residual dipolar couplings with violations less than 1 Hz and 2 residual dipolar couplings with violations greater than 1 Hz compared with the experimentally observed residual dipolar couplings.

Analysis of Structures with CURVES 5.3

The helical parameters of the decoding site in the 30S subunit-paromomycin crystal structure and the original and residual dipolar coupling-refined decoding site oligonucleotide-paromomycin NMR structures were generated with the computer program CURVES 5.3 [30]. The protocol involved calculating the best straight helical axis for each of the two A form stems flanking the asymmetric internal loop in the decoding site defined. Stem 1 was defined as the C1403-U1498, C1404-G1497, and G1405-C1496 base pairs, and stem 2 was defined as the C1409-G1491, G1410-C1490, C1411-G1489, and C1412-G1488 base pairs in the crystal structure. The corresponding base pairs were used to define stem 1 and stem 2 in the NMR structures. The two straight helix axes were then used to measure the interhelical bend angle for each structure.

Acknowledgments

The authors would like to thank Prof. Ignacio Tinoco, in whose laboratory the Pf1 bacteriophage purification and calculation protocols for structure refinement against residual dipolar couplings were initiated.

This work was supported by NIH grant GM51266. The Stanford Magnetic Resonance Laboratory is supported by the Stanford School of Medicine.

Received: June 20, 2002
Revised: October 9, 2002
Accepted: October 9, 2002

References

1. Moazed, D., and Noller, H.F. (1987). Interaction of antibiotics with functional sites in 16S ribosomal RNA. Nature *327*, 389–394.
2. Woodcock, J., Moazed, D., Cannon, M., Davies, J., and Noller, H.F. (1991). Interaction of antibiotics with A- and P-site-specific bases in 16S ribosomal RNA. EMBO J. *10*, 3099–3103.
3. Moazed, D., and Noller, H.F. (1986). Transfer RNA shields specific nucleotides in 16S ribosomal RNA from attack by chemical probes. Cell *47*, 985–994.
4. Davies, J., Gorini, L., and Davis, B.D. (1965). Misreading of RNA codewords induced by aminoglycoside antibiotics. Mol. Pharmacol. *1*, 93–106.
5. Edelmann, P., and Gallant, J. (1977). Mistranslation in E. coli. Cell *10*, 131–137.
6. Karimi, R., and Ehrenberg, M. (1994). Dissociation rate of cognate peptidyl-tRNA from the A-site of hyper-accurate and error-prone ribosomes. Eur. J. Biochem. *226*, 355–360.
7. Pape, T., Wintermeyer, W., and Rodnina, M.V. (2000). Conformational switch in the decoding region of 16S rRNA during aminoacyl-tRNA selection on the ribosome. Nat. Struct. Biol. *7*, 104–107.
8. Recht, M.I., Fourmy, D., Blanchard, S.C., Dahlquist, K.D., and Puglisi, J.D. (1996). RNA sequence determinants for aminoglycoside binding to an A-site rRNA model oligonucleotide. J. Mol. Biol. *262*, 421–436.
9. Fourmy, D., Recht, M.I., Blanchard, S.C., and Puglisi, J.D. (1996). Structure of the A site of E. coli 16S ribosomal RNA complexed with an aminoglycoside antibiotic. Science *274*, 1367–1371.
10. Yoshizawa, S., Fourmy, D., and Puglisi, J.D. (1998). Structural origins of gentamicin antibiotic action. EMBO J. *17*, 6437–6448.
11. Fourmy, D., Yoshizawa, S., and Puglisi, J.D. (1998). Paromomycin binding induces a local conformational change in the A site of 16S rRNA. J. Mol. Biol. *277*, 333–345.
12. Yoshizawa, S., Fourmy, D., and Puglisi, J.D. (1999). Recognition of the codon-anticodon helix by ribosomal RNA. Science *285*, 1722–1725.
13. Carter, A.P., Clemons, W.M., Jr., Brodersen, D.E., Morgan-Warren, R.J., Wimberly, B.T., and Ramakrishnan, V. (2000). Functional insights from the structure of the 30S ribosomal subunit and its interactions with antibiotics. Nature *407*, 340–348.
14. Wimberly, B.T., Brodersen, D.E., Clemons, W.M., Jr., Morgan-Warren, R.J., Carter, A.P., Vonrhein, C., Hartsch, T., and Ramakrishnan, V. (2000). Structure of the 30S ribosomal subunit. Nature *407*, 327–339.
15. Vicens, Q., and Westhof, E. (2001). Crystal structure of paromomycin docked into the eubacterial ribosomal decoding A site. Structure *9*, 647–658.
16. Ogle, J.M., Brodersen, D.E., Clemons, W.M., Jr., Tarry, M.J., Carter, A.P., and Ramakrishnan, V. (2001). Recognition of cognate transfer RNA by the 30S ribosomal subunit. Science *292*, 897–902.
17. Brünger, A.T. (1990). X-Plor Manual. (New Haven, CT.: Yale University).
18. Brünger, A.T., Adams, P.D., Clore, G.M., DeLano, W.L., Gros, P., Grosse-Kunstleve, R.W., Jiang, J.S., Kuszewski, J., Nilges, M., Pannu, N.S., et al. (1998). Crystallography and NMR system: a new software system for macromolecular structure determination. Acta Crystallogr. *D54*, 905–921.
19. Gutell, R.R. (1994). Collection of small subunit (16S- and 16S-like) ribosomal RNA structures: 1994. Nucleic Acids Res. *22*, 3502–3507.
20. Recht, M.I., Douthwaite, S., and Puglisi, J.D. (1999). Basis for prokaryotic specificity of action of aminoglycoside antibiotics. EMBO J. *18*, 3133–3138.
21. Lynch, S.R., and Puglisi, J.D. (2001). Structural origins of aminoglycoside specificity for prokaryotic ribosomes. J. Mol. Biol. *306*, 1037–1058.
22. Puglisi, J.D., and Wyatt, J.R. (1995). Biochemical and NMR studies of RNA conformation with an emphasis on RNA pseudoknots. Methods Enzymol. *261*, 323–350.
23. Clore, G.M., Bax, A., Driscoll, P.C., Wingfield, P.T., and Gronenborn, A.M. (1990). Assignment of the side-chain 1H and 13C resonances of Interleukin-1b using double- and triple-resonance heteronuclear three-dimensional NMR spectroscopy. Biochemistry *29*, 8172–8184.
24. Nikonowicz, E.P., and Pardi, A. (1992). Three-dimensional heteronuclear NMR studies of RNA. Nature *355*, 184–186.
25. Marino, J.P., Schwalbe, H., Anklin, C., Bermel, W., Crothers, D.M., and Griesinger, C. (1994b). A three-dimensional triple-resonance 1H, 13C, 31P experiment: sequential through-bond correlation of ribose protons and intervening phosphorus along the RNA oligonucleotide backbone. J. Am. Chem. Soc. *116*, 6472–6473.
26. Sklénar, V., Miyashiro, H., Zon, G., and Bax, A. (1986). Assignment of the ^{31}P and ^{1}H resonances in oligonucleotides by two-dimensional NMR spectroscopy. FEBS Lett. *208*, 94–98.
27. Marino, J.P., Prestegard, J.H., and Crothers, D.M. (1994). Correlation of adenine H2/H8 resonances in uniformly ^{13}C labeled RNAs by 2D HCCH-TOCSY: a new tool for ^{1}H assignment. J. Am. Chem. Soc. *116*, 2205–2206.
28. Wimberly, B., Varani, G., and Tinoco, I., Jr. (1993). The conformation of loop E of eukaryotic 5S ribosomal RNA. Biochemistry *32*, 1078–1087.
29. Losonczi, J.A., Andrec, M., Fischer, M.W., and Prestegard, J.H. (1999). Order matrix analysis of residual dipolar couplings using singular value decomposition. J. Magn. Reson. *138*, 334–342.
30. Lavery, R., and Sklenar, H. (1988). The definition of generalized helicoidal parameters and of axis curvature for irregular nucleic acids. J. Biomol. Struct. Dyn. *6*, 63–91.